Magnetic field generation from bubble collisions during first-order phase transition

Jing Yang
Department of physics, Chongqing University, Chongqing 401331, China

Ligong Bian*
Department of Physics and Chongqing Key Laboratory for Strongly Coupled Physics, Chongqing University, Chongqing 401331, People's Republic of China and Center for High Energy Physics, Peking University, Beijing 100871, China

(Received 18 May 2022; accepted 8 July 2022; published 15 July 2022)

We study the magnetic field generation from the cosmological first-order electroweak phase transition. We calculate the magnetic fields induced by the variation of the Higgs phase for two-bubble and three-bubble collisions, and find that the generated magnetic field strength with the effect of bubble shape distortion is about half of that derived without including the shape deformation. Our study shows that electromagnetic currents in the collision direction produce the ringlike magnetic field in the intersection area of colliding bubbles, which has a chance to seed the primordial magnetic field constrained by intergalactic magnetic field observations.

DOI: 10.1103/PhysRevD.106.023510

I. INTRODUCTION

Though observations have established the existence of cosmological magnetic fields (MFs), their origin is still a long-standing unsolved problem. The MFs may generate during inflation [1], and/or electroweak phase transition [2]. The MFs from the electroweak first-order phase transition (FOPT) may seed the intergalactic MFs [3]. The phase transition in the Standard Model (SM) is a *crossover* [4], and the electroweak FOPT is a general prediction of many models beyond the SM, e.g., the SM extended by the dimensional-six operator $(\Phi^\dagger\Phi)^3/\Lambda^2$ [5,6], singlet extension of the SM [7–15], two-Higgs-doublet models [16–21], George-Macheck model [22], and next-to minimal supuersymmetric model [23,24]. Therefore, measurements of intergalactic MFs may provide an additional way to probe physics beyond the SM [25,26]. We refer to Refs. [25,27–30] for previous reviews on the primordial MFs. For the status of the observation of MFs in the Galaxy, we refer to Ref. [31].

A FOPT proceeds with vacuum bubbles' nucleation and collision. In analogy with Kibble and Vilenkin [32], Ahonen and Enqvist [33] studied ringlike MF generation during the collision process of bubbles within an Abelian Higgs model. They evaluated the root-mean-square MFs to be around 10^{-21} G at the comoving scale of 10 Mpc today after including turbulent enhancement effects. Stevens *et al.* [34] studied the MFs created from the currents induced by the charged W fields for the two-bubble collision scenario, and they further considered the effect of bubble wall thickness in Ref. [35]. Recently, they utilized the thermal erasure principle to solve the equation of motion (EOM) of electromagnetic fields in the non-Abelian Higgs model, and found that the strength of the MFs for the two-bubble collision is comparable to those found in the Abelian Higgs model; see Ref. [36]. Different from previous studies, in this work, we take into account the effects of the bubble dynamics during the FOPT, i.e., the different dynamics between the bubble walls in the cross regions of bubbles and other regions induced by the thermal frictions and bubble wall tension. We consider the MF generation by bubble collisions during the electroweak FOPT. For concreteness and simplicity, we consider the MF generation for two- and three-bubble collisions. Here, with and without considering bubble dynamics, are called the *ideal situation* and *revised situation*. The prospect for constraining the electroweak FOPT with MF observation is studied.

This work is organized as follows. In Sec. II, we demonstrate the dynamics of bubble collision. In Sec. III, we calculate the MFs of electroweak bubble collisions in the ideal and the revised situation. In Sec. IV, we evaluate the root-mean-squared MFs at correlation length after taking into account the hydromagnetic turbulent effect, and evaluate the possibility to probe the electroweak FOPT with Blazars observation. We conclude with Sec. V. In Appendix, we review the EOMs for the W and Z fields, and how one can derive the electromagnetic current by solving the Higgs phase equation and estimate the produced MFs during the bubble collision process.

*lgbycl@cqu.edu.cn

II. BUBBLE DYNAMICS

In the thin-wall limit, the Lagrangian of the vacuum bubble is a function of the bubble radius R and can be written as [37]

$$L = -4\pi\sigma R^2\sqrt{1-\dot{R}^2} + \frac{4\pi}{3}R^3 p, \tag{1}$$

where σ is the bubble wall tension and p is the pressure acting on the bubble wall. The EOM to describe bubble growth is given by

$$\ddot{R} + 2\frac{1-\dot{R}^2}{R} = \frac{p}{\sigma}(1-\dot{R}^2)^{\frac{3}{2}}. \tag{2}$$

In terms of Lorentz factor γ, the above equation recasts the form of

$$\frac{d\gamma}{dR} + \frac{2\gamma}{R} = \frac{p}{\sigma}, \tag{3}$$

where $\gamma \equiv 1/\sqrt{1-\dot{R}^2}$. It can be solved analytically by giving an initial condition of γ and R. The smallest bubble size of the case where bubbles would expand instead of collapsing after nucleating is $R_c = 2\sigma/p$.

When the bubbles are expanding in the plasma background, the friction force can be exerted by the surrounding plasma. In the case where the bubble wall is very relativistic, the leading-order friction is caused by the change of the effective mass during the $1 \to 1$ particle transmission and reflection in the vicinity of the bubble wall, which is independent of the Lorentz factor γ, and is estimated to be [38]

$$\Delta P_{\rm LO} \approx \frac{\Delta m^2 T^2}{24}, \tag{4}$$

with the squared masses differences between the symmetric phase and the broken phase being given by

$$\Delta m^2 \equiv \sum_i c_i N_i \Delta m_i^2. \tag{5}$$

Where, N_i is the number of internal degrees of freedom of particles, $c_i = 1(1/2)$ for bosons(fermions), $\Delta m_i^2 = m_{i,t}^2 - m_{i,f}^2$ is the mass difference of particles in the true vacuum ("t") and the false vacuum ("f"), and the sum running over particles that gain mass in the transition from the false vacuum to the true vacuum. The next-to-leading order term arising from the particle splitting and transition radiation of gauge bosons is proportional to γ [39]:

$$\gamma\Delta P_{\rm NLO} \approx g^2 \Delta m_V T^3, \tag{6}$$

with

$$g^2\Delta m_V \equiv \sum_{i\in V} g_i^2 N_i \Delta m_i, \tag{7}$$

where the sum running over all gauge bosons with its masses changing across the wall ($\Delta m_i = m_{i,t} - m_{i,f}$), and the g_i are their gauge couplings. After these frictions are included, the total pressure can be written as

$$p \equiv \Delta V - \Delta P_{\rm LO} - \gamma\Delta P_{\rm NLO}, \tag{8}$$

with $\Delta V = V_f - V_t$ being the energy density difference between the false vacuum and the true vacuum. Equation (3) becomes [40]

$$\frac{d\gamma}{dR} + \frac{2\gamma}{R} = \frac{\Delta P_{\rm NLO}}{\sigma}(\gamma_{\rm eq} - \gamma). \tag{9}$$

Here, $\gamma_{\rm eq} = (\Delta V - \Delta P_{\rm LO})/(\Delta P_{\rm NLO})$ and $\lim_{R\to\infty}\gamma(R) = \gamma_{\rm eq}$ [41]. We assume $\Delta P_{\rm NLO} \gg \sigma$ which means the bubble wall accelerated rapidly after nucleation, therefore the Lorentz factor of the bubble wall can be approximately evaluated as $\gamma_{\rm col} \approx \gamma_{\rm eq}$ when the bubble collision started.

Based on above arguments, when the bubble collision occurs, the bubbles' walls outside the cross regions can be described by Eq. (9), and bubbles expand with a constant velocity where $\gamma \sim \gamma_{\rm eq}$. Meanwhile, we have $p \equiv 0$ in the cross region of colliding bubbles. Assuming Eqs. (3) and (9) still hold in these regions, we get

$$\frac{d\gamma}{dR} + \frac{2\gamma}{R} = 0, \tag{10}$$

with the solution being

$$\gamma = \gamma_{\rm col}\frac{R_{\rm col}^2}{R^2}, \tag{11}$$

where $R_{\rm col}$ is the radius of the bubble and $\gamma_{\rm col}$ is the Lorentz factor of the bubble wall at the collision time $t_{\rm col}$. For the following calculations of the modified MFs' strength, we take $\gamma_{\rm col} = \gamma_{\rm eq}$.

At the time of $t' \equiv t - t_{\rm col} = t_m$, the points on the bubble wall along the collision axis reach the maximum distance away from the bubble center with $R_{\rm col}m_W = 10$. We show the shape of the bubble walls with solid lines in the left panel of Fig. 1 (which corresponds to the revised situation in the right panel). Here we introduce an angle to describe the position of the points on the wall; the distance between the wall and bubble center is related to the angle down from the collision axis, i.e., ϕ. The bubble wall with different ϕ begins to intersect with that of the other bubble at different times. Therefore, in the cross regions, the distance between the points on bubble walls and the bubble center depends on the angle (ϕ) and the time after collision. Equation (10) applies until the moment when the points on the bubble wall with an angle ϕ reach the maximum

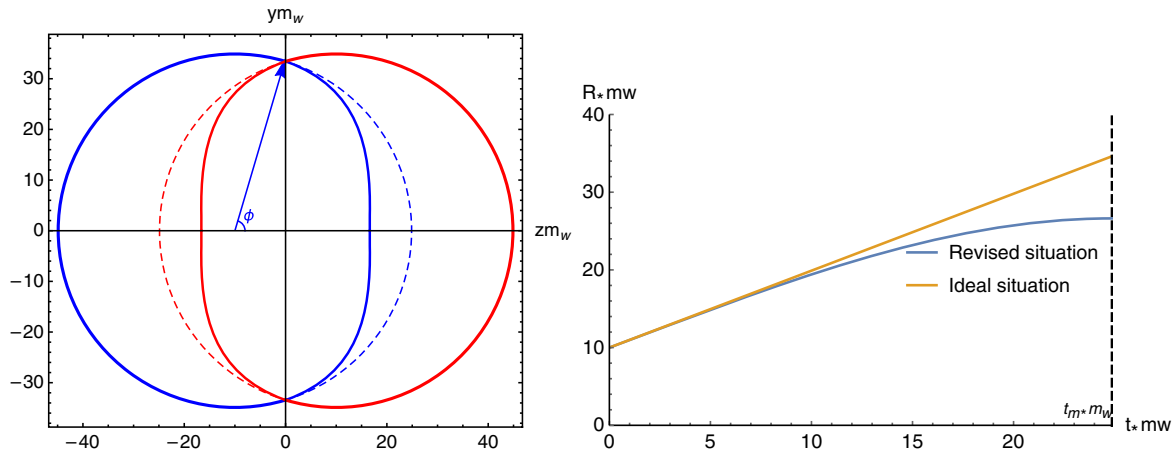

FIG. 1. Left: The shape of the two bubbles after collision at time $t' \equiv t - t_{\rm col} = t_m$ is shown with thick lines. The dashed lines are the case where $\gamma \equiv \gamma_{\rm eq}$ is always satisfied on the whole bubble walls. Right: The time dependence of the distance between the bubble center and the point of the bubble walls along the collision axis in the cross region is shown in the right panel. The blue line represents the revised situation and the orange one describes the ideal situation.

distance. Meanwhile, the bubble wall outside the intersection area still expands with a velocity $\gamma = \gamma_{\rm eq}$. The dashed lines are plotted to describe the ideal case which is adopted to evaluate the MFs in the previous study of Ref. [36]. As shown in the figure, the bubble walls are straightened by their tension force and result in a larger curvature radius in the cross region, thus yielding a deviation of bubble shapes from the ideal case where the bubble shapes are both spheres. In the right panel, we plot the time evolution of the radius of bubble walls in the intersection area for the revised and the ideal situation. The kinetic energy of bubble walls in the intersection area is converted to the wall surface energy due to the surface tension, thus leading to the decelerated expansion of bubble walls in the revised situation rather than a uniform expansion velocity as in the ideal situation.

III. MAGNETIC FIELD PRODUCTION

For the Higgs potential with proper barrier for quantum tunneling at finite temperature around $\mathcal{O}(10^2)$ GeV can feasibly be an electroweak FOPT proceeding with bubble nucleation and collision [5], and therefore yields production of the MFs [25,29,30]. In unitary gauge, the Higgs field has the form

$$\Phi(x) = \begin{pmatrix} 0 \\ \rho(x)\exp(i\Theta(x)) \end{pmatrix}. \tag{12}$$

It was found that the fluctuations in $\rho(x)$ became very small as the bubbles overlapped [34], thus we take $\rho(x) = \rho_0 = 174$ GeV in our calculations where ρ_0 is a central value of $\rho(x)$. For the EOMs of Higgs and gauge fields, see Appendix.

As indicated in Eq. (A14), when bubbles collide there would be a large gradient of the Higgs phase since different bubbles may have different Higgs phases, and, consequently, a large electromagnetic current and a large MF will be generated [as indicated by Eqs. (A16) and (A17)]. In the following, we take into account the bubble dynamics as explored in the previous section, and calculate the strength of the MFs generated by two-bubble collisions and three-bubble collisions.

A. Collision of two bubbles

The simplest case is that two bubbles nucleate simultaneously; one bubble locates at $(t, x, y, z) = (0, 0, 0, vt_{\rm col})$, and the other one locates at the position of $(t, x, y, z) = (0, 0, 0, -vt_{\rm col})$. Since our calculations of the MFs are only relevant to the $v_{\rm col}$ and $R_{\rm col}$, we suppose they are expanding with the same uniform velocity v and neglect their initial nucleating radius for simplicity. The system under study has an $O(2)$ symmetry in the spatial coordinate, we therefore follow the analysis of Kibble and Vilenkin [32] and express the EOM in a coordinate (τ, z) which has an $O(1,2)$ symmetry when $v = 1$. To obtain the MFs generated by the bubbles' collision, we need to solve the equation of the Higgs field phase Θ, i.e., Eq. (A15). In the (τ, z) coordinate, it casts the form of

$$\left(\frac{v^2+1}{\tau} + \frac{v^2(1-v^2)t^2}{\tau^3}\right)\frac{\partial\Theta}{\partial\tau} + \left(1 + \frac{v^2(v^2-1)t^2}{\tau^2}\right)\frac{\partial^2\Theta}{\partial\tau^2} - \frac{\partial^2\Theta}{\partial z^2} = 0, \tag{13}$$

where $\tau \equiv \sqrt{v^2t^2 - r^2}$ with $r^2 \equiv x^2 + y^2$. Note that $0 \le r \le \sqrt{v^2t^2 - R_{\rm col}^2}$ in the cross region, where $\sqrt{v^2t^2 - R_{\rm col}^2}$ is the radius of the circular intersection area in the x-y plane at $z = 0$, which also indicates $R_{\rm col} \le \tau \le vt$. If we assume $r \ll vt$ or $v \approx 1$, the equation recasts the form

$$\frac{2}{\tau}\frac{\partial\Theta}{\partial\tau}+v^2\frac{\partial^2\Theta}{\partial\tau^2}-\frac{\partial^2\Theta}{\partial z^2}=0. \tag{14}$$

We assume that before the bubble collision occurs, the Higgs phase for a single bubble is constant throughout the bubble and the two bubbles have different phases. As in [33], the boundary conditions of Θ are given by

$$\Theta(\tau=t_{\rm col},z)=\Theta_0\epsilon(z),\frac{\partial}{\partial\tau}\Theta(\tau=t_{\rm col},z)=0, \tag{15}$$

where $\epsilon(z)$ is the sign of z and $0<\Theta_0<\pi/2$. Expressing $\Theta(x)$ as a Fourier transform in z, the above equation gives a τ-depend ordinary differential equation, yielding,

$$\Theta(\tau,z)=\frac{1}{\sqrt{2\pi}}\int_{-\infty}^{\infty}dke^{ikz}\left(a_k\tau^{\frac{-2+v^2}{2v^2}}K_1\left(\frac{-2+v^2}{2v^2},\frac{\omega_k\tau}{v}\right)+b_k\tau^{\frac{-2+v^2}{2v^2}}K_2\left(\frac{-2+v^2}{2v^2},\frac{\omega_k\tau}{v}\right)\right), \tag{16}$$

where $\omega_k=\sqrt{k^2+m^2}$, K_1 and K_2 are the Bessel functions of the first and second kind, respectively, a_k and b_k are determined by the boundary conditions of Θ. When we take $m\to 0$, the solution can be obtained. Then, from Eq. (A14), the $j_\nu^{\rm em}(\tau,z)$ takes the form

$$j_\nu^{\rm em}(\tau,z)=(j_z(\tau,z),x_\alpha j(\tau,z)), \tag{17}$$

with

$$j_z=-\frac{g'}{g}\sqrt{g^2+g'^2}\rho_0^2\frac{\partial}{\partial z}\Theta(\tau,z), \tag{18}$$

$$j=-\frac{g'}{g}\sqrt{g^2+g'^2}\rho_0^2\frac{1}{\tau}\frac{\partial}{\partial\tau}\Theta(\tau,z), \tag{19}$$

and $x_\alpha=(vt,-x,-y)$. It is clear that the electromagnetic field has the same form as the electromagnetic current,

$$A_\nu^{\rm em}(\tau,z)=(a_z(\tau,z),x_\alpha a(\tau,z)). \tag{20}$$

Taking the axial gauge $a_z=0$, Maxwell's equation becomes [36]

$$-\frac{\partial^2}{\partial z^2}a(\tau,z)=j(\tau,z). \tag{21}$$

Applying the boundary conditions, namely, $a(\tau,-\infty)=0$, and $\partial_z a(\tau,-\infty)=0$, we obtain

$$a(\tau,z)=-\int_{-\infty}^{z}dz'\int_{-\infty}^{z'}j(\tau,z'')dz''. \tag{22}$$

With which, and apply Eq. (A17), we get the MF,

$$B^z=0,\quad B^x=-y\int_{-\infty}^{z}j(\tau,z')dz',\quad B^y=x\int_{-\infty}^{z}j(\tau,z')dz'. \tag{23}$$

When $v=1$, Eq. (16) reduces to

$$\Theta(\tau,z)=\frac{\Theta_0}{\tau}\theta(T-|z|)z+\Theta_0\epsilon(z)\theta(|z|-T), \tag{24}$$

where $T=\tau-t_{\rm col}$. Then, the j takes the form

$$j=\frac{g'}{g}\sqrt{g^2+g'^2}\rho_0^2\frac{\Theta_0}{\tau^3}\theta(T-|z|)z. \tag{25}$$

Finally, we get

$$\vec{B}=\frac{(-y,x,0)}{r}B^\phi, \tag{26}$$

with

$$B^\phi=r\frac{g'}{g}\sqrt{g^2+g'^2}\rho_0^2\frac{\Theta_0}{\tau^3}\theta(T-|z|)\times\frac{|z|^2-T^2}{2}. \tag{27}$$

It is clear to see that the largest MF strength is in the $z=0$ plane. With the increase of the r, r/τ^3 would become larger while T^2 would decrease and $T^2=0$ at the largest $r=\sqrt{v^2t^2-R_{\rm col}^2}$, we therefore expect the largest MF strength appears near the largest r when two bubbles collide, which grows after the time of bubble collision ($t_{\rm col}$). This reason yields a ringlike distribution of the created MFs close to the walls of the colliding bubbles.

1. Equal bubbles-ideal situation

We first consider that the two colliding bubbles are of equal size. In Fig. 2, we show the configuration of the Θ for $v=0.5$ and $v=1$ as a function of the distance z along the axis of collision for different τm_W, where the collision radius is $R_{\rm col}m_W\equiv vt_{\rm col}m_W=10$. We find there is only a slight difference between the cases of $v=0.5$ and $v=1$ for the same τm_W. Thus the MFs strength from the bubble collisions for the two cases have a similar profile as shown in Fig. 3. At a distance $rm_W=1$ and $\tau m_W=20$, 30, 40, and 50, the magnitude of the MFs are of order $\sim 0.01m_W^2$. It can be seen that near the center of the overlap region at $z=r=0$, the MFs are much smaller than the region near $\tau=R_{\rm col}$, and the MFs have a tendency to drop at fixed r when the overlap region grows.

The magnitude of the MFs in the x-y plane is shown in Fig. 4. The figure shows that the large magnitude of the MFs almost distributes near the edge of the overlap region, which indicates that the produced MF is of a ringlike

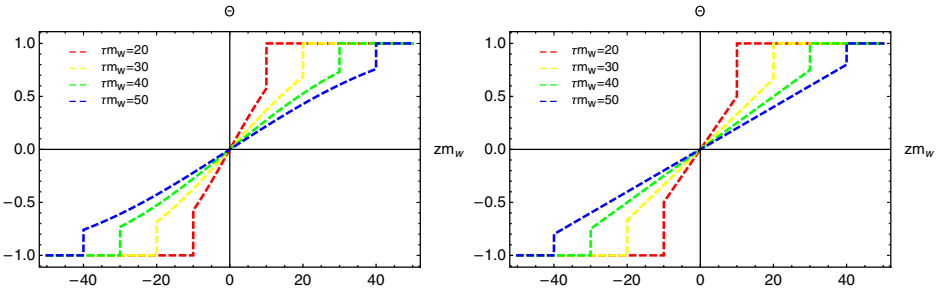

FIG. 2. Higgs phase Θ is shown as a function of the distance z for $\tau m_W = 20, 30, 40, 50$, with $\Theta_0 = 1$. In the left panel, we plot the case of $v = 0.5, t_{\rm col} m_W = 20$. In the right panel, we consider the case of $v = 1, t_{\rm col} m_W = 10$.

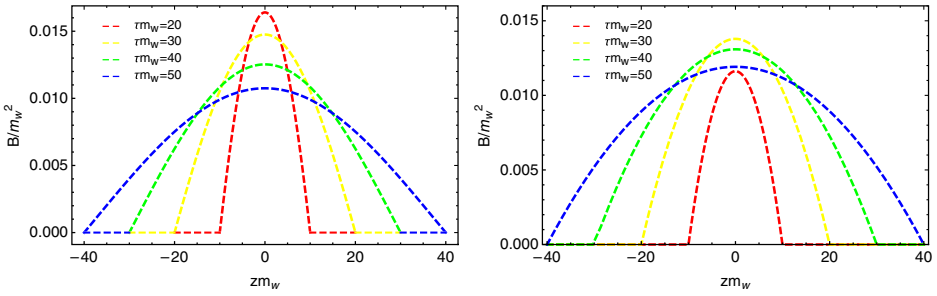

FIG. 3. Magnitude of the MFs for two-bubble collisions. The strength of the MFs is shown as a function of the distance z along the axis of collision at a distance $rm_W = 1$ from the axis of collision for $\tau m_W = 20$, 30, 40, and 50. Left: we consider the case $v = 0.5, t_{\rm col} m_W = 20$. Right: we consider the case $v = 1, t_{\rm col} m_W = 10$.

distribution. This feature confirms the discussions under Eq. (27).

2. *Unequal bubbles-ideal situation*

Then, we turn to the unequal bubble collision situation, where the two bubbles nucleate at two different moments. For simplicity, we consider two bubbles are nucleated at $(t_1, x_1, y_1, z_1) = (0, 0, 0, -d_1)$ and $(t_2, x_2, y_2, z_2) = (d_1 - d_2, 0, 0, d_2)$, where $d_1 > d_2 > 0$. We consider the case where they expand at a velocity $v \equiv 1$ after nucleating, so they would collide at $z = 0, t = d_1$. We find nucleation events have a spacelike interval due to $\Delta x^\mu \Delta x_\mu = (d_1 - d_2)^2 - (d_1 + d_2)^2 < 0$. Therefore, one can use an appropriate Lorentz boost to obtain a frame in which the two bubbles are nucleated simultaneously [43]. In the new frame after the boost, the coordinates (t'', x'', y'', z'') have the form of

$$t'' = \gamma(t - \Delta v \cdot x), \qquad x'' = x, \qquad y'' = y,$$
$$z'' = \gamma(z - \Delta v \cdot t), \tag{28}$$

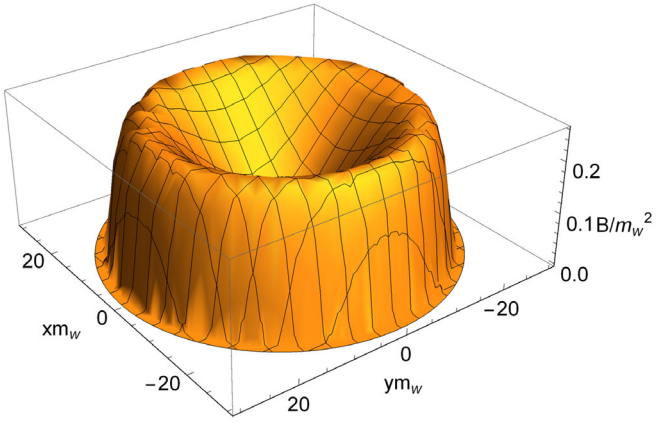

FIG. 4. Magnitude of the MFs for two-bubble collision in the x-y plane for $z = 0$ at the time of $tm_W = 30$ for $v = 1$ and $t_{\rm col} m_W = 10$.

where Δv is the velocity of the new frame relative to the old one. The condition that two bubbles nucleate simultaneously requires $t_1'' = t_2''$, so we get $\Delta v = (d_1 - d_2)/(d_1 + d_2)$.

We take $d_1 m_W = 2 d_2 m_W = 20$, and calculate the MFs in the new frame using Eq. (27). In order to get the final result, we perform a Lorentz transformation of the MFs obtained above back to the old frame. Figure 5 shows the bubbles' shape for unequal bubble collisions where nucleations occur at $(t_1, x_1, y_1, z_1) = (0, 0, 0, -2d)$ and $(t_2, x_2, y_2, z_2) = (d, 0, 0, d)$ (see the left panel) and the produced MFs are in the old frame (see the right panel). The figure shows that MFs at different times are peaked at points with different coordinate z, and depicts an asymmetry between the left-hand side and right-hand side of

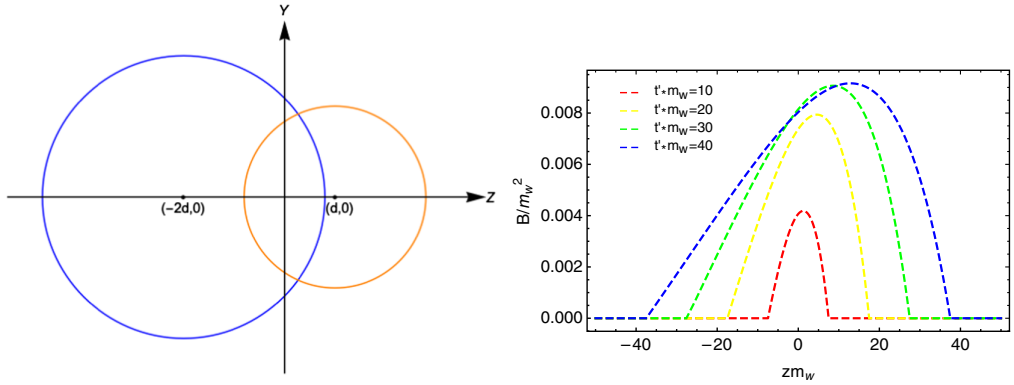

FIG. 5. Left: Bubble shapes for unequal bubbles' collision. Right: MFs generated by unequal bubbles' collision. The field is shown at time $t'm_W \equiv (t - t_{\rm col})m_W = 10$, 20, 30, 40 after collision, in which we consider $v = 1$, $dm_W = 10$, $rm_W = 1$.

peaks since unequal bubble collision breaks the $O(1,2)$ and Z_2 symmetries in spacetime.

3. Equal bubbles-revised situation

So far, we have calculated the MFs generated by a two-bubble collision in an ideal case where the velocity of the whole bubbles is unchanged after the collision, and the bubbles are of perfect spherical shapes. While, in the realistic situation, the velocity of the intersecting bubble walls may change due to the bubble tension, which leads to a deviation of the bubbles' shape; see Sec. II for details. When the friction force is considered, the bubble wall velocity can never reach 1; however, we found that the solution of the MFs is not very sensitive to the v. Thus if v is very close to 1, we can approximately take $v = 1$ in our calculations of the MFs. For an illustration, we suppose that bubbles expand with a velocity $v = v_{\rm eq} = 0.99$ after they nucleated, and the radius of the two bubbles at the collision time are both $R_{\rm col}m_W = 10$. To solve Eq. (14) by using the boundary conditions Eq. (15), we make an assumption that the solution of Θ is still nearly proportional to z in the cross region as shown in Fig. 2. It is easy to find that z/τ_0 is a solution to Eq. (14) at $v = 1$, where $\tau = \tau_0 = \sqrt{t^2 - r^2}$. We can approximately take $\tau_{\rm col} = \sqrt{v_{\rm col}^2 t^2 - r^2} \approx \tau_0$. Thus the general solution takes the form

$$\Theta(\tau_0, \tau(t,r), z) = C_1(\tau(t,r)) * \frac{z}{\tau_0} + C_2(\tau(t,r)). \quad (29)$$

Then, we fix C_1 and C_2 by using the boundary condition Eq. (15) and considering that in the region without intersection one has a constant phase $\pm\Theta_0$. Considering the distance between the bubble wall and the bubble center $R(t,r)$ is a function of $r = \sqrt{x^2 + y^2}$ and the time after collision is $t - t_{\rm col}$ in the cross region, we introduce $\tau(t,r) = \sqrt{R(t,r)^2 - r^2}$ in our solutions to reflect the influence of bubble shapes on boundary condition, the phase in the region without intersection is then given by $\pm\Theta_0$. We found the solution is

$$\Theta(\tau_0, \tau(t,r), z) = \frac{\Theta_0}{\tau_0}\theta(T(t,r) - |z|)z + \Theta_0\epsilon(z)\theta(|z| - T(t,r)), \quad (30)$$

where $T(t,r) = \tau(t,r) - R_{\rm col}$. By using this solution of Θ, we found the strength of MFs in the revised situation takes the form

$$B^\phi = r\frac{g'}{g}\sqrt{g^2 + g'^2}\rho_0^2\frac{\Theta_0}{\tau_0^3}\theta(T(t,r) - |z|) \times \frac{|z|^2 - T(t,r)^2}{2}. \quad (31)$$

We use this equation to evaluate the strength of MFs in the following.

To demonstrate the difference between the revised and the ideal situation, in Fig. 6, we show the MFs as a function of distance z along the axis of collision with $rm_w = 1$. We consider the time $t - t_{\rm col} = t_m$ when the points on bubble walls along the collision axis reach the maximum distance with bubble center in the revised situation. The MFs strength in the revised situation is nearly half of the

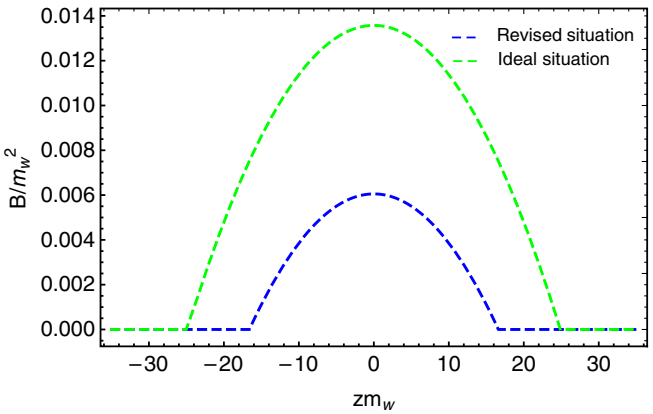

FIG. 6. The MF strength is shown as a function of the distance z along the axis of collision with $rm_W = 1$, where $v_{\rm col} = 0.99$, $R_{\rm col}m_W = 10$. Blue dashed and green dashed lines indicate the revised and ideal situations, respectively.

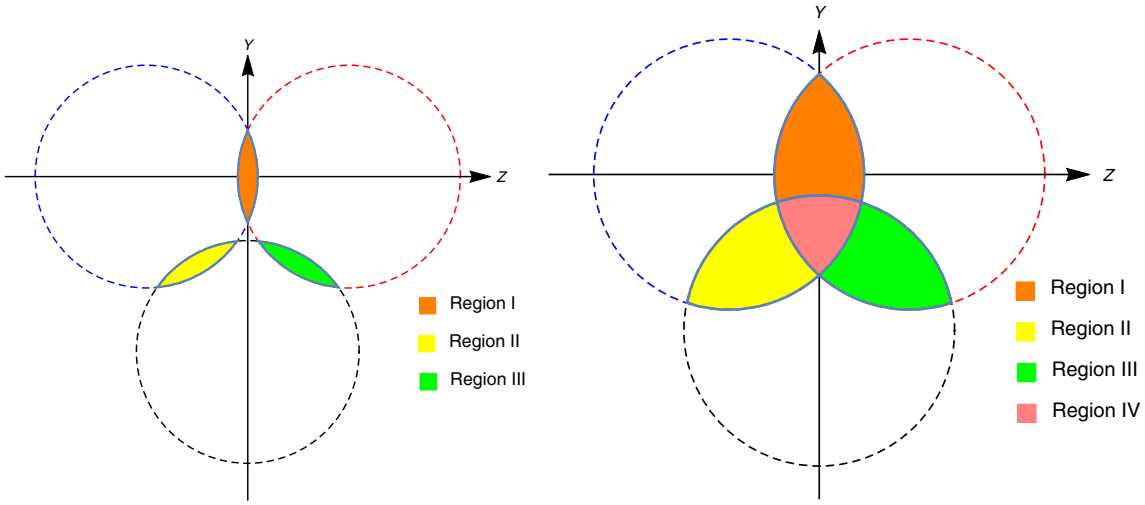

FIG. 7. Left: cross regions of three bubbles in the y-z plane at $t - t_{\rm col} = 0.1R_{\rm col}$; Right: cross regions of three bubbles in the y-z plane at $t - t_{\rm col} = 0.5R_{\rm col}$.

magnitude in the ideal situation, and the distribution area of the MFs in the revised situation is smaller than the ideal situation. As in Eqs. (27) and (31), $B \propto T^2 - |z|^2$, where $T = \tau - R_{\rm col} = \sqrt{v^2t^2 - r^2} - R_{\rm col}$ in the ideal situation, in the revised situation $T = T(t,r) = \tau(t,r) - R_{\rm col} = \sqrt{R(t,r)^2 - r^2} - R_{\rm col}$ instead. In the intersection area, $|z| \leq T$ which means the MFs strength generated in the ideal situation is larger than the revised situation due to $vt > R(t,r)$ at the same z, r, and t. The results are consistent with the bubbles' shape after the collision as shown in Fig. 1. Since the intersection area of bubbles in the revised situation is smaller than the ideal situation, the electromagnetic current distributes in a smaller area and therefore causes a lower strength of the MFs.

B. Collision of three bubbles

In this section, we consider that three equal size bubbles nucleate simultaneously. We consider they expand at the same velocity with $\gamma_{\rm col} = \gamma_{\rm eq}$ and then collide with each other at the same time. The simplest case is that one bubble nucleates at $(t,x,y,z) = (0,0,0,-R_{\rm col})$ and other two nucleate at $(0,0,0,R_{\rm col})$ and $(0,0,-\sqrt{3}R_{\rm col},0)$, respectively. At first, there would be three regions where they overlap in pairs. After a period, three regions may overlap and there will be a region (at the center of three bubbles) bounded by the intersection of the three bubbles. We show the cross regions of three-bubble collision in Fig. 7. We can imagine that the MFs strength of the region IV can be represented by the superposition of the other three regions. For $v = 0.99 \approx 1$, we take $\tau = \tau_0 = \sqrt{t^2 - r^2}$ for simplicity. We set the phases of the three bubbles as $\Theta_1 = 0$, $\Theta_2 = \frac{2\pi}{3}$, and $\Theta_3 = \frac{4\pi}{3}$, we choose the center of region I to be the original point, the initial conditions can now be written as follows.

Region I:

$$\Theta(\tau = t_{\rm col}, z) = \frac{\Theta_1 - \Theta_2}{2}\epsilon(z) + \frac{\Theta_1 + \Theta_2}{2},$$
$$\Theta'(\tau = t_{\rm col}, z) = 0,$$
$$\tau = \sqrt{t^2 - x^2 - y^2}. \tag{32}$$

Region II:

$$\Theta\left(\tau' = t_{\rm col}, \frac{1}{2}(z - t_{\rm col}) - \frac{\sqrt{3}}{2}y\right)$$
$$= \frac{\Theta_3 - \Theta_2}{2}\epsilon\left(\frac{1}{2}(z - t_{\rm col}) - \frac{\sqrt{3}}{2}y\right) + \frac{\Theta_2 + \Theta_3}{2},$$
$$\Theta'\left(\tau' = t_{\rm col}, \frac{1}{2}(z - t_{\rm col}) - \frac{\sqrt{3}}{2}y\right) = 0,$$
$$\tau' = \sqrt{t^2 - x^2 - \left(\frac{\sqrt{3}}{2}(z + t_{\rm col}) + \frac{1}{2}y\right)^2}. \tag{33}$$

Region III:

$$\Theta\left(\tau'' = t_{\rm col}, -\frac{1}{2}(z + t_{\rm col}) - \frac{\sqrt{3}}{2}y\right)$$
$$= \frac{\Theta_3 - 2\pi - \Theta_1}{2}\epsilon\left(-\frac{1}{2}(z + t_{\rm col}) - \frac{\sqrt{3}}{2}y\right)$$
$$+ \frac{\Theta_3 + 2\pi + \Theta_1}{2},$$
$$\Theta'\left(\tau'' = t_{\rm col}, -\frac{1}{2}(z + t_{\rm col}) - \frac{\sqrt{3}}{2}y\right) = 0,$$
$$\tau'' = \sqrt{t^2 - x^2 - \left(\frac{\sqrt{3}}{2}(z - t_{\rm col}) - \frac{1}{2}y\right)^2}. \tag{34}$$

And the MFs of these three regions can be solved similarly, with

Region I

$$B^x = -yB_1,$$
$$B^y = xB_1,$$
$$B^z = 0. \tag{35}$$

Region II

$$B^x = -(y - \sqrt{3}z - \sqrt{3}t_{\rm col})\frac{B_2}{2},$$
$$B^y = \frac{x}{2}B_2,$$
$$B^z = -\frac{\sqrt{3}}{2}xB_2. \tag{36}$$

Region III

$$B^x = -(y + \sqrt{3}z - \sqrt{3}t_{\rm col})\frac{B_3}{2},$$
$$B^y = \frac{x}{2}B_3,$$
$$B^z = \frac{\sqrt{3}}{2}xB_3. \tag{37}$$

Region IV

$$B^x = -yB_1 - (y - \sqrt{3}z - \sqrt{3}t_{\rm col})\frac{B_2}{2} - (y + \sqrt{3}z - \sqrt{3}t_{\rm col})\frac{B_3}{2},$$
$$B^y = xB_1 + x\frac{B_2}{2} + x\frac{B_3}{2},$$
$$B^z = \frac{\sqrt{3}}{2}x(B_3 - B_2), \tag{38}$$

where

$$B_1 = \frac{g'}{g}\sqrt{g^2 + g'^2}\rho_0^2\frac{\Theta_1 - \Theta_2}{\tau^2}\theta(\tau - t_{\rm col} - |z|)\frac{|z|^2 - (\tau - t_{\rm col})^2}{2},$$
$$B_2 = \frac{g'}{g}\sqrt{g^2 + g'^2}\rho_0^2\frac{\Theta_3 - \Theta_2}{\tau'^2}\theta\left(\tau' - t_{\rm col} - \left|\frac{1}{2}(z - t_{\rm col}) - \frac{\sqrt{3}}{2}y\right|\right)\frac{\left|\frac{1}{2}(z - t_{\rm col}) - \frac{\sqrt{3}}{2}y\right|^2 - (\tau' - t_{\rm col})^2}{2},$$
$$B_3 = \frac{g'}{g}\sqrt{g^2 + g'^2}\rho_0^2\frac{\Theta_3 - \Theta_1 - 2\pi}{\tau''^2}\theta\left(\tau'' - t_{\rm col} - \left|\frac{1}{2}(z + t_{\rm col}) + \frac{\sqrt{3}}{2}y\right|\right)\frac{\left|\frac{1}{2}(z + t_{\rm col}) + \frac{\sqrt{3}}{2}y\right|^2 - (\tau'' - t_{\rm col})^2}{2}.$$

Note that the solutions are only valid in the cross regions. After $t > \frac{2}{\sqrt{3}}t_{\rm col}$, three regions may overlap with each other, and the MFs in region IV are the superposition of the other three regions.

1. Three equal bubbles-ideal situation

For illustration, we show the strength of the MFs induced by three-bubble collision at $t - t_{\rm col} = 0.1R_{\rm col}$ and $t - t_{\rm col} = t_m$ in the y-z plane in Fig. 8. We can see that the MF

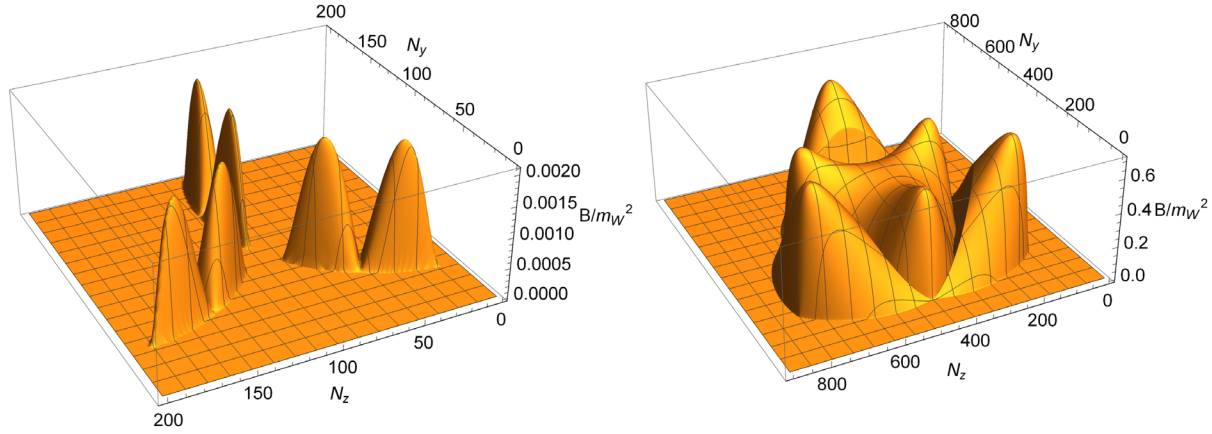

FIG. 8. Magnitude of the MFs (in the ideal situation) produced by three-bubble collision for $v = 0.99, R_{\rm col}m_w = t_{\rm col}m_W = 10$. We show the MFs as a function of lattice numbers N_y and N_z on y and z axes, respectively, with lattice spacing $a = 0.1/m_W$. Left panel: Magnitude of the MFs at $x = 0, t - t_{\rm col} = 0.1R_{\rm col}$. Right panel: Magnitude of the MFs at $x = 0, t - t_{\rm col} = t_m$.

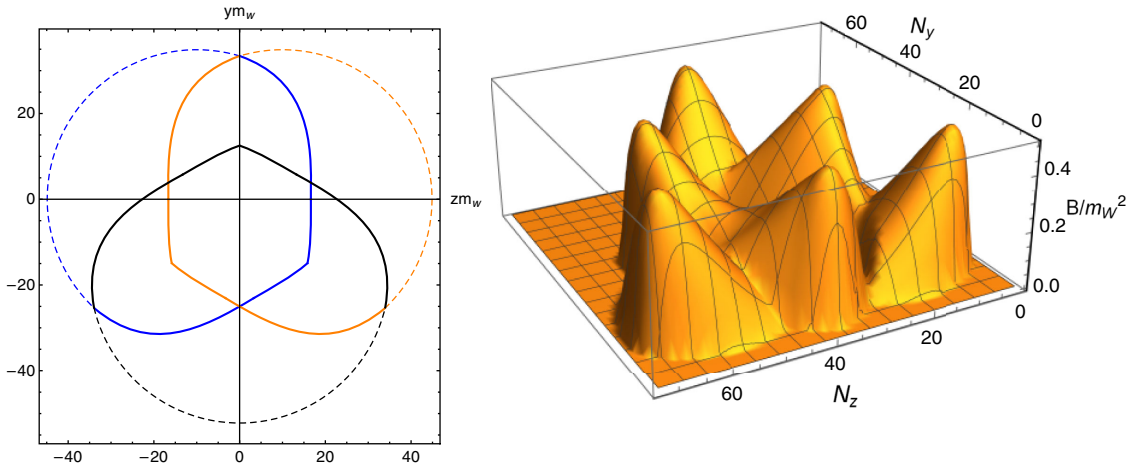

FIG. 9. Left panel: The shape of three bubbles after collision at $t - t_{\rm col} = t_m$ for $v = 0.99$ and $R_{\rm col} m_W = 10$. Right panel: Magnitude of the MFs produced by three-bubble collision. The MFs in the revised situation is shown as a function of lattice numbers N_y and N_z on the y and z axes, respectively, with lattice spacing $a = 1/m_W$ at $x = 0, t - t_{\rm col} = t_m$.

distribution of the three regions are separated as expected (see the left panel), where the peak of MF strength is distributed on the symmetric axis of the overlap region. At a latter time of $t - t_{\rm col} = t_m$, the three regions would overlap and the MFs are continuously distributed (see the right panel). The magnitude of the MFs is nearly *zero* in the vicinity of the center of the cross regions. And the strength of the MFs in region IV is of the same order as other three regions.

2. Three equal bubbles-revised situation

While taking into consideration the real bubble collision dynamics, the cross regions of the three-bubble collision would be revised as shown in Fig. 9. The bubbles shape and the MFs generation of three-bubble collision are calculated at $(x = 0, t - t_{\rm col} = t_m)$ with $v_{\rm col} = 0.99$ and $R_{\rm col} m_W = 10$. In comparison with the ideal situation as shown in Fig. 8, the magnitude of the MFs strength in the revised situation is shown to be nearly half of the ideal situation, and the MFs distribute more continuously.

IV. IMPLICATION FOR COSMOLOGICAL OBSERVATION

The comoving Hubble length at the electroweak phase transition temperature T_* is given by [44]

$$\lambda_{H_*} = 5.8 \times 10^{-10}\ {\rm Mpc}(100\ {\rm GeV}/T_*)(100/g_*)^{1/6}, \quad (39)$$

where g_* is the number of relativistic degrees of freedom at the moment when the MF is generated. The comoving correlation length for the primordial MF at the generation time can be evaluated to be

$$\xi_\star = \Gamma \lambda_{H_*}. \quad (40)$$

Here, Γ is the factor to account for bubble numbers inside one Hubble radius at the FOPT, and $\Gamma \simeq 0.01$ for the electroweak FOPT occurring with phase transition duration $\sim\mathcal{O}(10^2)$. For recent simulations, see Refs. [45,46].

The physical MF amplitudes scale with the expansion of the Universe as

$$B_* = \left(\frac{a_*}{a_0}\right)^2 B, \quad (41)$$

with the time-temperate relation being

$$\frac{a_*}{a_0} \simeq 8 \times 10^{-16}(100\ {\rm GeV}/T_*)(100/g_*)^{1/3}. \quad (42)$$

The simulation of the evolution of hydromagnetic turbulence from the electroweak phase transition until recombination suggests that the root-mean-squared nonhelical MF amplitude and the correlation length satisfies the following relation [47],

$$B_{\rm rms} = B_* \left(\frac{\xi}{\xi_*}\right)^{-(\beta+1)/2}, \quad (43)$$

where $\beta = 1$, 2, and 4 for nonhelical case, with ξ being the magnetic correlation length. For illustration, we show in Fig. 10 the bounds of Blazars spectra on the MF strength at variant correlation lengths, which depicts that the $\beta = 1$ case is allowed by the data. Here we consider the equal bubbles-ideal situation and the equal bubbles-revised situation for two-bubble collision; the MFs are generated at $z = 0$ with the r ($r \sim 3R_{\rm col}$), where the largest MF strength appears at $t(= t_m + t_{\rm col})$ and we have the ringlike distribution of the MFs. And the strength of the MFs generated in the revised situation is about half of which is generated in the ideal situation. The MF strength here is almost the same

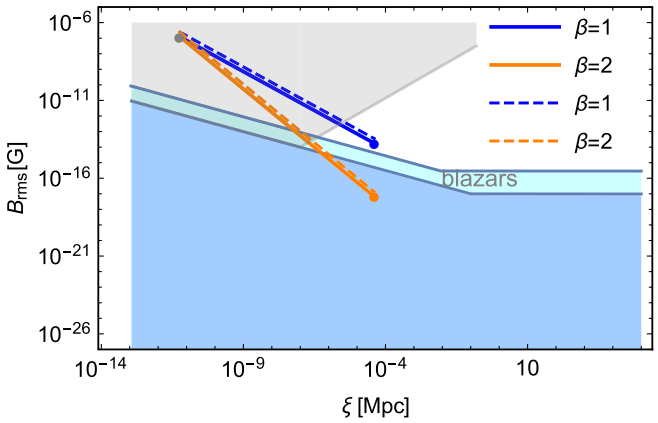

FIG. 10. MF strength $B_{\rm rms}$ at the correlation length ξ calculated for the two-bubble collision of the equal bubbles-ideal situation (dashed lines) and equal bubbles-revised situation (solid lines). Gray region shows the upper bound on the MF strength adopting from Fig. 9 of Ref. [48], which is derived by Ref. [57]. Cyan and blue regions are plotted to consider the bounds set by Blazars given in Ref. [58] and Ref. [48].

for the three-bubble collision. Considering the effects of the turbulent magnetohydrodynamics on the MFs generated before the recombination, the upper bounds on the MF strength are shown in Fig. 10 in the gray region, which excludes the scenarios of $B_{\rm rms} \geq 10^{-11}$ G for $\xi \sim 10^{-4}$ Mpc [48] and yield null constraints on the two situations under study. Primordial MFs suffer bounds from big bang nucleosynthesis [49,50] and the measurements of the spectrum and anisotropies of the cosmic microwave background [51–56], these limits yield null bounds on the parameter space under study in this work.

V. CONCLUSIONS AND DISCUSSIONS

We study the dynamics of bubbles in this work and we found that the bubble walls are straightened in the bubbles' cross regions that yield a deviation of bubble shapes from spheres. Then we use the EOMs of gauge fields to calculate the MFs generated during the bubble collisions stage at the electroweak FOPT. After obtaining the Higgs phases when bubbles collide with each other, we calculate the MFs strength after obtaining the electromagnetic current and apply the approach to the situations of two-bubble and three-bubble collisions, equal and unequal bubbles, ideal and revised situations under the assumption that $\gamma_{\rm col} = \gamma_{\rm eq}$. We find that the electroweak bubble collisions produce the ringlike MF distributions when we consider the revised situation with bubble walls deviating from the spherical shape. For that situation, we get a slightly lower MF strength because the electromagnetic current is distributed in a smaller area. The scaling law resulting from the hydromagnetic turbulence after the electroweak FOPT suggests that this kind of MF under study can be probed by the observation of the intergalactic MF. The MF strength calculated here is comparable with the MF generated from the bubble collisions simulation performed in Refs. [45,46].

We remind the readers that, for the scenario where bubbles collide shortly after nucleating if they are randomly generated close to each other, the bubbles' radius and velocity would be relatively smaller at the collision time, and the Lorentz factor of bubbles does not have enough time to reach $\gamma_{\rm eq}$, which indicates that the assumption of this study does not hold. For that scenario, one have to conduct numerical studies as in Refs. [45,46] by specifying different bubbles' nucleation rates at different spacetimes. We further note that, in the paradigm of the electroweak baryogenesis, the Chern-Simons connects the helicity of the MFs produced during bubble collision and the baryon asymmetry of the early Universe [3,59]. Therefore, the observation of the helicity of the primordial MFs may serve as a test of the electroweak baryogenesis. Reference [60] studied the primordial MF from first-order phase transition in the $B - L$ model and the SM extended by the dimensional-six operator $(\Phi^\dagger\Phi)^3/\Lambda^2$, with the physical implication that the observable gravitational waves and collider signatures would be complementary to the MFs observation from the first-order phase transitions when the inverse cascade process is taken into account for helical MFs [61–63].

ACKNOWLEDGMENTS

We thank Yi-Zen Chu, Francesc Ferrer, Jinlin Han, Marek Lewicki, Shao-Jiang Wang, Ke-Pan Xie, and Yiyang Zhang for useful communications and discussions. We appreciate the anonymous referee's constructive comments and suggestions. This work was supported by the National Natural Science Foundation of China under Grants No. 12075041, No. 12147102, and No. 12047564, and the Fundamental Research Funds for the Central Universities of China (No. 2021CDJQY-011, No. 2021CDJLXB001, and No. 2020CDJQY-Z003), and Chongqing Natural Science Foundation (Grants No. cstc2020jcyj-msxmX0814).

APPENDIX: EQUATION OF MOTIONS FOR GAUGE BOSONS

In this section, we review the derivation of the magnetic field from EOMs of gauge bosons. The relevant Lagrangian of electroweak bosonic fields is

$$L_{\rm EW} = L_1 + L_2 - V(\phi, T). \tag{A1}$$

Here, we consider the $V(\Phi, T)$ being the Higgs potential that can drive electroweak FOPT in frameworks beyond the SM and therefore can admit bubble expansion and collision as aforementioned. As in Ref. [36], we focus on the general feature of MF production from bubble collision in this study and left detailed studies of specific FOPT models for future work. The other two terms that are related in the calculation of MFs are given by

$$L_1 = -\frac{1}{4}W^i_{\mu\nu}W^{i\mu\nu} - \frac{1}{4}B_{\mu\nu}B^{\mu\nu},$$
$$W^i_{\mu\nu} = \partial_\mu W^i_\nu - \partial_\nu W^i_\mu - g\epsilon_{ijk}W^j_\mu W^k_\nu,$$
$$B_{\mu\nu} = \partial_\mu B_\nu - \partial_\nu B_\mu, \tag{A2}$$

and

$$L_2 = \left|\left(i\partial_\mu - \frac{g}{2}\tau\cdot W_\mu - \frac{g'}{2}B_\mu\right)\Phi\right|^2, \tag{A3}$$

where, τ_i is the $SU(2)$ generator. The physical Z and $A^{\rm em}_\mu$ fields are

$$A^{\rm em}_\mu = \frac{1}{\sqrt{g^2+g'^2}}(g'W^3_\mu + gB_\mu),$$
$$Z_\mu = \frac{1}{\sqrt{g^2+g'^2}}(gW^3_\mu - g'B_\mu), \tag{A4}$$

and the Higgs doublet takes the form of

$$\Phi(x) = \begin{pmatrix} 0 \\ \rho(x)\exp(i\Theta(x)) \end{pmatrix}, \tag{A5}$$

where $\Theta(x)$ is the phase of the Higgs field and $\rho(x)$ is its magnitude. For this choice of gauge, the EOM for the B field is

$$\partial^2 B_\nu - \partial_\nu\partial\cdot B + g'\rho(x)^2\psi_\nu(x) = 0, \tag{A6}$$

where the ψ_ν is

$$\psi_\nu(x) \equiv \partial_\nu\Theta - \frac{\sqrt{g^2+g'^2}}{2}Z_\nu, \tag{A7}$$

and satisfies

$$\partial_\nu(\rho(x)^2\psi_\nu(x)) = 0. \tag{A8}$$

For $i = 3$, the gauge field W^i satisfies the following equation:

$$\partial^2 W^3_\nu - \partial_\nu\partial\cdot W^3 - g\rho(x)^2\psi_\nu(x) = j^3_\nu(x), \tag{A9}$$

and, for $i = 1, 2$, we have

$$\partial^2 W^i_\nu - \partial_\nu\partial\cdot W^i + m_W(x)^2 W^i_\nu = j^i_\nu(x), \tag{A10}$$

where $m_W(x)^2 = g^2\rho(x)^2/2$ and $j^i_\nu(x)$ is

$$j^i_\nu(x) \equiv g\epsilon_{ijk}(W^k_\nu\partial\cdot W^j + 2W^j\cdot\partial W^k_\nu - W^j_\mu\partial_\nu W^{k\mu}) - g^2\epsilon_{klm}\epsilon_{ijk}W^j_\mu W^{l\mu}W^m_\nu. \tag{A11}$$

The EOM for $A^{\rm em}$ casts the form of

$$\partial^2 A^{\rm em}_\nu - \partial_\nu\partial\cdot A^{\rm em} = j^{\rm em}_\nu(x),$$

with

$$j^{\rm em}_\nu(x) = \frac{g'}{\sqrt{g^2+g'^2}}j^3_\nu(x). \tag{A12}$$

And, the EOM for the Z field is obtained as

$$\partial^2 Z_\nu - \partial_\nu\partial\cdot Z - \rho(x)^2\sqrt{g^2+g'^2}\psi_\nu(x) = \frac{g}{g'}j^{\rm em}_\nu(x). \tag{A13}$$

Utilizing the thermal erasure [36] of $\langle Z\rangle = 0$, and suppose $\rho(x) = \rho_0$, which applies to the thin-wall limit for bubble collisions. Applying the ensemble averaging to Eqs. (A8) and (A13), we get

$$\langle j^{\rm em}_\nu\rangle = -\frac{g'}{g}\sqrt{g^2+g'^2}\rho_0^2\times\partial_\nu\Theta(x), \tag{A14}$$
$$\partial^2\Theta(x) = 0. \tag{A15}$$

Consequently, Eq. (A12) recasts the form of the Maxwell equation,

$$\partial^2 A_\nu - \partial_\nu\partial\cdot A = j^{\rm em}_\nu(x) = -\frac{g'}{g}\sqrt{g^2+g'^2}\rho_0^2\times\partial_\nu\Theta(x). \tag{A16}$$

Due to the magnetic field $\vec{B} = \vec{\nabla}\times\vec{A}^{\rm em}$, we can calculate the strength of the magnetic field after obtaining the electromagnetic current through,

$$\nabla^2\vec{B} = \vec{\nabla}\times\vec{j}^{\rm em}. \tag{A17}$$

[1] M. S. Turner and L. M. Widrow, Phys. Rev. D **37**, 2743 (1988).
[2] T. Vachaspati, Phys. Lett. B **265**, 258 (1991).
[3] T. Vachaspati, Phys. Rev. Lett. **87**, 251302 (2001).
[4] M. D'Onofrio, K. Rummukainen, and A. Tranberg, Phys. Rev. Lett. **113**, 141602 (2014).
[5] C. Grojean, G. Servant, and J. D. Wells, Phys. Rev. D **71**, 036001 (2005).
[6] C. Grojean and G. Servant, Phys. Rev. D **75**, 043507 (2007).
[7] S. Profumo, M. J. Ramsey-Musolf, C. L. Wainwright, and P. Winslow, Phys. Rev. D **91**, 035018 (2015).

[8] R. Zhou, L. Bian, and H. K. Guo, Phys. Rev. D **101**, 091903 (2020).
[9] L. Bian, H. K. Guo, Y. Wu, and R. Zhou, Phys. Rev. D **101**, 035011 (2020).
[10] A. Alves, T. Ghosh, H. K. Guo, K. Sinha, and D. Vagie, J. High Energy Phys. 04 (2019) 052.
[11] S. Profumo, M. J. Ramsey-Musolf, and G. Shaughnessy, J. High Energy Phys. 08 (**2007**) 010.
[12] J. R. Espinosa, T. Konstandin, and F. Riva, Nucl. Phys. **B854**, 592 (2012).
[13] M. Jiang, L. Bian, W. Huang, and J. Shu, Phys. Rev. D **93**, 065032 (2016).
[14] K. P. Xie, J. High Energy Phys. 02 (2021) 090.
[15] W. Liu and K. P. Xie, J. High Energy Phys. 04 (2021) 015.
[16] J. M. Cline, K. Kainulainen, and M. Trott, J. High Energy Phys. 11 (2011) 089.
[17] G. C. Dorsch, S. J. Huber, and J. M. No, J. High Energy Phys. 10 (2013) 029.
[18] G. C. Dorsch, S. J. Huber, K. Mimasu, and J. M. No, Phys. Rev. Lett. **113**, 211802 (2014).
[19] J. Bernon, L. Bian, and Y. Jiang, J. High Energy Phys. 05 (2018) 151.
[20] J. O. Andersen, T. Gorda, A. Helset, L. Niemi, T. V. I. Tenkanen, A. Tranberg, A. Vuorinen, and D. J. Weir, Phys. Rev. Lett. **121**, 191802 (2018).
[21] K. Kainulainen, V. Keus, L. Niemi, K. Rummukainen, T. V. I. Tenkanen, and V. Vaskonen, J. High Energy Phys. 06 (2019) 075.
[22] R. Zhou, W. Cheng, X. Deng, L. Bian, and Y. Wu, J. High Energy Phys. 01 (2019) 216.
[23] L. Bian, H. K. Guo, and J. Shu, Chin. Phys. C **42**, 093106 (2018); **43**, 129101(E) (2019).
[24] S. J. Huber, T. Konstandin, G. Nardini, and I. Rues, J. Cosmol. Astropart. Phys. 03 (2016) 036.
[25] R. Durrer and A. Neronov, Astron. Astrophys. Rev. **21**, 62 (2013).
[26] T. Vachaspati, Phys. Rev. D **95**, 063505 (2017).
[27] D. Grasso and H. R. Rubinstein, Phys. Rep. **348**, 163 (2001).
[28] D. G. Yamazaki, T. Kajino, G. J. Mathew, and K. Ichiki, Phys. Rep. **517**, 141 (2012).
[29] A. Kandus, K. E. Kunze, and C. G. Tsagas, Phys. Rep. **505**, 1 (2011).
[30] K. Subramanian, Rep. Prog. Phys. **79**, 076901 (2016).
[31] J. L. Han, Annu. Rev. Astron. Astrophys. **55**, 111 (2017); J. L. Han, R. N. Manchester, W. van Straten, and P. Demorest, Astrophys. J. Suppl. Ser. **234**, 11 (2018); J. Xu and J. L. Han, Mon. Not. R. Astron. Soc. **486**, 4275 (2019).
[32] T. W. B. Kibble and A. Vilenkin, Phys. Rev. D **52**, 679 (1995).
[33] J. Ahonen and K. Enqvist, Phys. Rev. D **57**, 664 (1998).
[34] T. Stevens, M. B. Johnson, L. S. Kisslinger, E. M. Henley, W. Y. P. Hwang, and M. Burkardt, Phys. Rev. D **77**, 023501 (2008).
[35] T. Stevens and M. B. Johnson, Phys. Rev. D **80**, 083011 (2009).
[36] T. Stevens, M. B. Johnson, L. S. Kisslinger, and E. M. Henley, Phys. Rev. D **85**, 063003 (2012).
[37] L. Darmé, J. Jaeckel, and M. Lewicki, Phys. Rev. D **96**, 056001 (2017).
[38] D. Bodeker and G. D. Moore, J. Cosmol. Astropart. Phys. 05 (2009) 009.
[39] D. Bodeker and G. D. Moore, J. Cosmol. Astropart. Phys. 05 (2017) 025.
[40] J. Ellis, M. Lewicki, J. M. No, and V. Vaskonen, J. Cosmol. Astropart. Phys. 06 (2019) 024.
[41] We note that the equation is revised in Ref. [42] with an additional correction for γ^2-dependent friction.
[42] R. G. Cai and S. J. Wang, J. Cosmol. Astropart. Phys. 03 (2021) 096.
[43] A. Kosowsky, M. S. Turner, and R. Watkins, Phys. Rev. D **45**, 4514 (1992).
[44] T. Kahniashvili, A. G. Tevzadze, A. Brandenburg, and A. Neronov, Phys. Rev. D **87**, 083007 (2013).
[45] Y. Zhang, T. Vachaspati, and F. Ferrer, Phys. Rev. D **100**, 083006 (2019).
[46] Y. Di, J. Wang, R. Zhou, L. Bian, R. G. Cai, and J. Liu, Phys. Rev. Lett. **126**, 251102 (2021).
[47] A. Brandenburg, T. Kahniashvili, S. Mandal, A. Roper Pol, A. G. Tevzadze, and T. Vachaspati, Phys. Rev. D **96**, 123528 (2017).
[48] A. M. Taylor, I. Vovk, and A. Neronov, Astron. Astrophys. **529**, A144 (2011).
[49] M. Kawasaki and M. Kusakabe, Phys. Rev. D **86**, 063003 (2012).
[50] T. Kahniashvili, A. G. Tevzadze, S. K. Sethi, K. Pandey, and B. Ratra, Phys. Rev. D **82**, 083005 (2010).
[51] T. R. Seshadri and K. Subramanian, Phys. Rev. Lett. **103**, 081303 (2009).
[52] P. A. R. Ade *et al.* (Planck Collaboration), Astron. Astrophys. **594**, A19 (2016).
[53] K. Jedamzik, V. Katalinic, and A. V. Olinto, Phys. Rev. Lett. **85**, 700 (2000).
[54] J. D. Barrow, P. G. Ferreira, and J. Silk, Phys. Rev. Lett. **78**, 3610 (1997).
[55] R. Durrer, P. G. Ferreira, and T. Kahniashvili, Phys. Rev. D **61**, 043001 (2000).
[56] P. Trivedi, K. Subramanian, and T. R. Seshadri, Phys. Rev. D **82**, 123006 (2010).
[57] R. Banerjee and K. Jedamzik, Phys. Rev. D **70**, 123003 (2004).
[58] M. Ackermann *et al.* (Fermi-LAT Collaboration), Astrophys. J. Suppl. Ser. **237**, 32 (2018).
[59] C. J. Copi, F. Ferrer, T. Vachaspati, and A. Achucarro, Phys. Rev. Lett. **101**, 171302 (2008).
[60] J. Ellis, M. Fairbairn, M. Lewicki, V. Vaskonen, and A. Wickens, J. Cosmol. Astropart. Phys. 09 (2019) 019.
[61] J. M. Cornwall, Phys. Rev. D **56**, 6146 (1997).
[62] M. Giovannini and M. E. Shaposhnikov, Phys. Rev. Lett. **80**, 22 (1998).
[63] H. Ji, Phys. Rev. Lett. **83**, 3198 (1999).